Dynamic Motion Control of Multi-Segment Soft Robots Using Piecewise Constant Curvature Matched with an Augmented Rigid Body Model

Robert K. Katzschmann*,1, Cosimo Della Santina*,1,2, Yasunori Toshimitsu[1], Antonio Bicchi[2,3], Daniela Rus[1]

***Abstract*— Despite the emergence of many soft-bodied robotic systems, model-based feedback control for soft robots has remained an open challenge. This is largely due to the intrinsic difficulties in designing controllers for systems with infinite dimensions. This work extends our previously proposed formulation for the dynamics of a soft robot from two to three dimensions. The formulation connects the soft robot's dynamic behavior to a rigid-bodied robot with parallel elastic actuation. The matching between the two systems is exact under the hypothesis of Piecewise Constant Curvature. Based on this connection, we introduce a control architecture with the aim of achieving accurate curvature and bending control. This controller accounts for the natural softness of the system moving in three dimensions, and for the dynamic forces acting on the system. The controller is validated in a realistic simulation, together with a kinematic inversion algorithm. The paper also introduces a soft robot capable of three-dimensional motion, that we use to experimentally validate our control strategy.**

I. Introduction

Animals interact robustly, compliantly, and continuously with the external world through their body's elasticity, and they perform dynamic tasks efficiently. Rigid robots move very different to animals, lacking most of these capabilities. Researcher have therefore take inspiration from nature and design soft robots with elastic bodies [1] and deformable actuation mechanisms, for example adaptive soft grippers [2], soft octopuses [3], and soft robotic fish [4].

Creating robots with soft bodies promises machines with great motion agility and compliance – such motion requires a *soft robotic brain* to compute the control for the soft body. Soft robotic systems have to robustly manage the intelligence embedded in their complex structure in order to generate reliable and repeatable behaviors. Substantial progress has been made in the development of soft robotic bodies, but developing control strategies suited for soft body control has remained particularly challenging [5]. Part of the difficulty is to create an exact mathematical formulation for the soft robotic model, which requires taking into account the infinite dimensionality of the robot's state space [6].

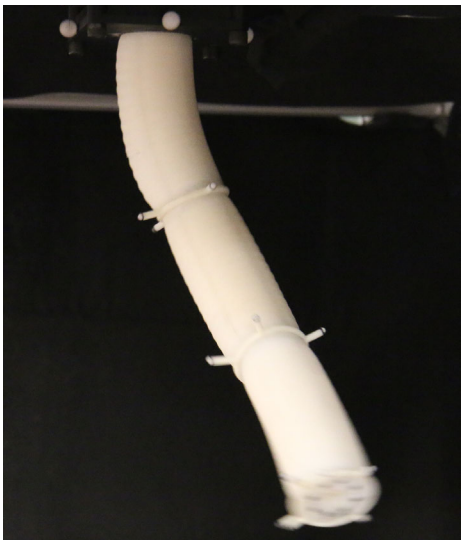

Fig. 1. Dynamically controlled soft robot following a desired trajectory. This soft robot arm consists of three segments and each segment has four individually addressable pneumatic chambers that deform under pressurization. The soft arm is controlled through a model-based feedback controller described in this paper.

The theory of infinite state space control is still confined to relatively simple systems, and its applications are still preliminary [7]. The use of learning techniques was considered as a possible alternative in [8], [9]. However, model-based techniques have an important role in achieving higher levels of performance in the control of both artificial and natural systems. This observation drove the development of simplified models capable of describing the robot's behavior through a finite set of variables. Several works focused on reduced descriptions of the soft robot's kinematics. Using such models, several quasi-static control strategies were proposed. Finite element methods (FEM) are the most natural way to achieve this goal. FEM-based kinematic models were used to design an algorithm for kinematic inversion [10] and planning [11]. However, a reduced kinematic model most commonly used in soft robotics kinematic control is the so-called *Piecewise Constant Curvature (PCC)* [12], [13]. The use of purely kinematic strategies for soft robot control, together with heuristically tuned low-level high gain feedback controllers, works well in static situations. However, a dynamic model is required for control strategies for dynamic tasks. Prior work on dynamic models with finite dimensions includes the Ritz-Galerkin models [14], and the discrete

*The authors contributed equally.

[1]Authors are with the Computer Science and Artificial Intelligence Laboratory, Massachusetts Institute of Technology, 32 Vassar St., Cambridge, MA 02139, USA, robert@katzschmann.de, yasu313nori@gmail.com, rus@csail.mit.edu

[2]Authors are with Centro E. Piaggio, University of Pisa, Italy, cosimodellasantina@gmail.com

[3]Author is with Soft Robotics for Human Cooperation and Rehabilitation, Fondazione Istituto Italiano di Tecnologia, via Morego, 30, 16163 Genova, Italy, antonio.bicchi@iit.it

Cosserat models [15], [16]. We are not aware of any prior work that applies these dynamic models to controlling soft robotics. Dynamic models based on the PCC hypothesis were presented in [17] and [18]. In both works, the models are merely used for generating purely feed-forward actuations.

In this work we propose a feedback control architectures that has been specifically designed for controlling soft multiple segments robots, extending our previous work from two to three dimensions [19], [20]. The proposed architectures is able to compensate for dynamical forces, while using the intelligence embodied in the soft body to stabilize a desired trajectory in the curvature space. The controller achieves regulation of time-varying curvatures profiles in free space. The proposed control scheme is based on an "augmented formulation" linking the soft robot to a classic rigid serial manipulator with a parallel elastic mechanism. Prior tools developed for rigid bodied robots can be used with this formulation [21].

To effectively test our architecture we designed and fabricated a new pneumatically actuated soft robot, depicted in Fig. 7. The arm is made of silicone, and has three actuated segments, with four chambers per segment. It is a soft limb realized through the ribbed design we introduced in [4].

This work contributes:

- a closed loop dynamic controller for a continuous soft robot capable of dynamically tracking desired curvatures in three dimensions.
- an "augmented formulation" linking a soft robot to a classic rigid serial manipulator under the Piecewise Constant Curvature hypothesis in three dimensions.
- simulations and experiments validating the controller on a 3D system.
- a 3D soft robot with an innovative design.

II. Background: Piecewise Constant Curvature Kinematics

We give a brief introduction to Piecewise Constant Curvature robots kinematics. Please refer to [12] for a more complete survey on this topic.

A Piecewise Constant Curvature (PCC) robot, is a mechanical system composed by a sequence of a fixed number of segments continuously deformable with curvature constant in space (CC) but variable in time, merged so that the resulting curve is everywhere differentiable. Fig. 2 presents an example of a soft robot composed by three CC segments. Consider a PCC robot composed by n CC segments. We introduce n reference frames $\{S_1\}, \dots, \{S_n\}$ attached at the ends of each segment, plus one base frame $\{S_0\}$. The knowledge of S_{i-1} and S_i fully define the configuration of the $i-th$ segment. Therefore, we describe the robot's kinematics by n homogeneous transformations $T_0^1, \dots, T_{n-1}^n$, which map each reference system to the subsequent one.

Fig. 3(a) shows the kinematics of a single CC segment. Two variables are sufficient to describe the segment's configuration under the hypothesis of non-extensibility, i.e. the angle ϕ_i between the plane $\hat{n}_{i-1} - \hat{o}_{i-1}$ and the plane on which the curvature occurs, and the relative rotation

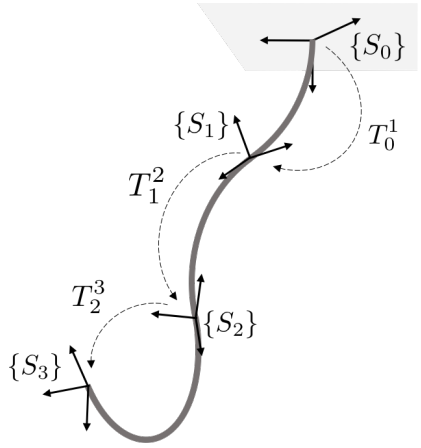

Fig. 2. Example of a 3D Piecewise Constant Curvature robot, composed by three constant curvature elements. $\{S_0\}$ is the robot's base frame. A reference frame $\{S_i\}$ is attached at the end of each segment. T_{i-1}^i is the homogeneous transformation mapping $\{S_{i-1}\}$ into $\{S_i\}$.

θ_i between the two reference systems expressed on that plane. Note that this angle is directly related to the segment curvature ρ_i through the linear relation $\theta_i\,\rho_i = L_i$, where L_i is the constant length of a segment. For this reason we will refer to θ_i as angle of curvature, or more simply as curvature. In the following we refer to $q_i = [\phi_i \ \theta_i]^{\mathrm{T}} \in \mathbb{R}^2$ as configuration of the $i-th$ segment. $q \in \mathbb{R}^n$ is the robot configuration and it collects q_i for all the n segments.

The $i-$th homogeneous transformation can be derived using geometrical considerations as

$$T_{i-1}^i(\phi_i, \theta_i) = R_z(\phi_i) \begin{bmatrix} R_y(\theta_i) & \rho_i(\theta_i) \begin{bmatrix} 1 - c_{\theta_i} \\ 0 \\ s_{\theta_i} \end{bmatrix} \\ \bar{0}_3 & 1 \end{bmatrix} R_z(-\phi_i)\ , \tag{1}$$

where $R_y(\theta_i)$ is a rotation around y of an angle θ_i, $R_z(\phi_i)$ is a rotation around z of an angle ϕ_i, $\rho_i(\theta_i)$ is the curvature radius, and c_{θ_i}, s_{θ_i} are $\cos(\theta_i)$, $\sin(\theta_i)$ respectively. The first rotation $R_z(\phi_i)$ has the role of changing the plane in which the curvature occurs. Follow a roto-translation implementing the curvature (the translation element can be derived through simple geometric considerations). Finally another rotation along the local vertical direction $\hat{a}_i$ is used for avoiding the introduction of not physical torsions of the arm (see [22] for more details).

The following homogeneous transformation results

$$T_{i-1}^i(\phi_i, \theta_i) = \begin{bmatrix} R_{i-1}^i(\phi_i, \theta_i) & t_{i-1}^i(\phi_i, \theta_i) \\ \bar{0}_3 & 1 \end{bmatrix}\ . \tag{2}$$

where

$$\begin{aligned} R_{i-1}^i &= \begin{bmatrix} \hat{x}_i & \hat{y}_i & \hat{z}_i \end{bmatrix} \\ &= \begin{bmatrix} c_{\phi_i}^2(c_{\theta_i} - 1) + 1 & s_{\phi_i} c_{\phi_i}(c_{\theta_i} - 1) & -c_{\phi_i} s_{\theta_i} \\ s_{\phi_i} c_{\phi_i}(c_{\theta_i} - 1) & c_{\phi_i}^2(1 - c_{\theta_i}) + c_{\theta_i} & -s_{\phi_i} s_{\theta_i} \\ c_{\phi_i} s_{\theta_i} & s_{\phi_i} s_{\theta_i} & c_{\theta_i} \end{bmatrix} \end{aligned} \tag{3}$$

and

$$t_{i-1}^i = \frac{L_i}{\theta_i} \begin{bmatrix} c_{\phi_i}(c_{\theta_i} - 1) & s_{\phi_i}(c_{\theta_i} - 1) & s_{\theta_i} \end{bmatrix}^{\mathrm{T}} \tag{4}$$

where c_{ϕ_i}, s_{ϕ_i}, c_{θ_i}, s_{θ_i} are respectively $\cos(\phi_i)$, $\sin(\phi_i)$, $\cos(\theta_i)$, $\sin(\theta_i)$.

III. Proposed model

The dynamic model of the PCC robot proposed here is an extension to three dimensions of our previous work describing a planar version [19], [20].

A. Equivalent Augmented Formulation of the i-th CC segment

In this section we propose a dynamic model of a generic serial PCC soft robot, using the *augmented formulation* framework. The basic idea of the framework is to introduce a classic rigid robot with a sufficient amount of degrees of freedom and a large enough operational space, for which always exists a configuration satisfying two constraints. The first one is of kinematic nature, i.e. placing its end effector frame on the end frame $\{S_{i-1}\}$ of a CC segment. The second one is of dynamic nature, i.e. a frame attached to one of the robot links must coincide with the CC segment's center of mass (CoM) reference frame.

A rigid robot satisfying only the kinematic constraint was proposed in [22] for the 3D case. It was composed as a sequence of five joints (RRPRR), where R stands for revolute and P for prismatic. [19] introduces an equivalent rigid robot satisfying both constraints for the planar case. It was composed as a sequence of four joints (RPPR).

To design such a robotic architecture for the 3D case, we start by defining for a CC segment the CoM position in space. Let us consider that each CC segment has a homogeneous mass distribution. Its center of mass is located on the line connecting the center of curvature with the middle of the arc, as shown in Fig.s 3(b) and 3(c). The distance between the CoM and the center of curvature is

$$a_i(\theta_i) = \rho_i \frac{\sin(\frac{\theta_i}{2})}{\frac{\theta_i}{2}} = 2L_i \frac{\sin(\frac{\theta_i}{2})}{\theta_i^2} \,, \tag{5}$$

where L_i is the $i-$th segment's length, ρ_i its curvature, and θ_i the correspondent degree of curvature. We do not report here the full derivation, which can be found in basic texts of continuous mechanics.

The rigid robot described by the Denavit-Hartenberg convention in Table I satisfies both constraints. Fig. 3(b) shows the robot superimposed to the CC segment for $\phi_i = 0$. The robot's configuration is described by the vector $\xi^i \doteq \begin{bmatrix}\xi_{10(i-1)+1} & \dots & \xi_{10(i-1)+10}\end{bmatrix}^{\mathrm{T}}$. First and last joints are a counterpart of the two coupled rotations in (1), implementing the change of plane of curvature by ϕ, and the correspondent inverse rotation to avoid the introduction of a phantom torsion. Fifth and sixth joints have a similar role of avoiding center of mass rotation due to the same effect. Second, third and fourth joints implement the planar transformation from $\{S_{i-1}\}$ to the center of mass. Seventh, eighth and ninth joint implement the planar transformation from the center of mass to the frame $\{S_i\}$.

TABLE I

Denavit-Hartenberg parametrization of a rigid robot matching both dynamics and kinematics of the i–th CC segment. The parameters θ, d, a, α refer to the classic DH parametrization, while μ refers to the mass.

Joint	θ	d	a	α	μ
1	$\xi_{10(i-1)+1}$	0	0	$-\frac{\pi}{2}$	0
2	$\xi_{10(i-1)+2}$	0	0	$\frac{\pi}{2}$	0
3	0	$\xi_{10(i-1)+3}$	0	$-\frac{\pi}{2}$	0
4	$\xi_{10(i-1)+4}$	0	0	$\frac{\pi}{2}$	0
5	$\xi_{10(i-1)+5}$	0	0	0	μ_i
6	$\xi_{10(i-1)+6}$	0	0	$-\frac{\pi}{2}$	0
7	$\xi_{10(i-1)+7}$	0	0	$\frac{\pi}{2}$	0
8	0	$\xi_{10(i-1)+8}$	0	$-\frac{\pi}{2}$	0
9	$\xi_{10(i-1)+9}$	0	0	$\frac{\pi}{2}$	0
10	$\xi_{10(i-1)+10}$	0	0	0	0

To complete the analysis we introduce a set of nonlinear constraints that, when satisfied, assure the matching between the augmented rigid configuration and the CC segment

$$\begin{bmatrix}\xi_{10(i-1)+1}\\ \xi_{10(i-1)+2}\\ \xi_{10(i-1)+3}\\ \xi_{10(i-1)+4}\\ \xi_{10(i-1)+5}\\ \xi_{10(i-1)+6}\\ \xi_{10(i-1)+7}\\ \xi_{10(i-1)+8}\\ \xi_{10(i-1)+9}\\ \xi_{10(i-1)+10}\end{bmatrix} = \begin{bmatrix}\phi_i\\ \frac{\theta_i}{2} - \eta_i(\theta_i)\\ b_i(\theta_i)\\ \eta_i(\theta_i)\\ -\phi_i\\ \phi_i\\ \eta_i(\theta_i)\\ b_i(\theta_i)\\ \frac{\theta_i}{2} - \eta_i(\theta_i)\\ -\phi_i\end{bmatrix} \doteq m_i(\phi_i, \theta_i) \tag{6}$$

where $b_i(\theta_i)$ and $\eta_i(\theta_i)$ are defined as in Fig. 3(c). They can be evaluated through simple trigonometric considerations, as

$$\begin{aligned} b_i(\theta_i) &= \sqrt{\left(\frac{L_i}{\theta_i}\sin\left(\frac{\theta_i}{2}\right)\right)^2 + \left(a_i(\theta_i) - \frac{L_i}{\theta_i}\cos\left(\frac{\theta_i}{2}\right)\right)^2} \\ &= \frac{L_i}{\theta_i}\sqrt{1 + 4\frac{\sin\left(\frac{\theta_i}{2}\right)}{\theta_i}\left(\frac{\sin\left(\frac{\theta_i}{2}\right)}{\theta_i} - \cos\left(\frac{\theta_i}{2}\right)\right)}\,, \end{aligned} \tag{7}$$

$$\eta_i(\theta_i) = \arccos\left(\frac{1}{b_i(\theta_i)}\frac{L_i}{\theta_i}\sin\left(\frac{\theta_i}{2}\right)\right) \,. \tag{8}$$

Note that the map $m_i(\phi_i, \theta_i)$ is well defined also in $\theta_i = 0$, where it holds

$$\lim_{\theta_i \to 0} b_i(\theta_i) = \frac{L_i}{2} \,, \quad \lim_{\theta_i \to 0} \eta_i(\theta_i) = 0 \,. \tag{9}$$

A generic PCC robot can be matched to a corresponding rigid structure by connecting in sequence several of the (RRPRRRRPRR) element introduced above. The augmented robot configuration is $\xi = [\xi^1 \dots \xi^n] \in \mathbb{R}^{10n}$. The set of nonlinear constraints assuring the equivalence between the augmented formulation and the PCC robot is $\xi = m(q)$, where $m(q)$ is defined as

$$m(q) = \begin{bmatrix}m_1(\phi_1, \theta_1)^T & \dots & m_n(\phi_n, \theta_n)^T\end{bmatrix}^T \,. \tag{10}$$

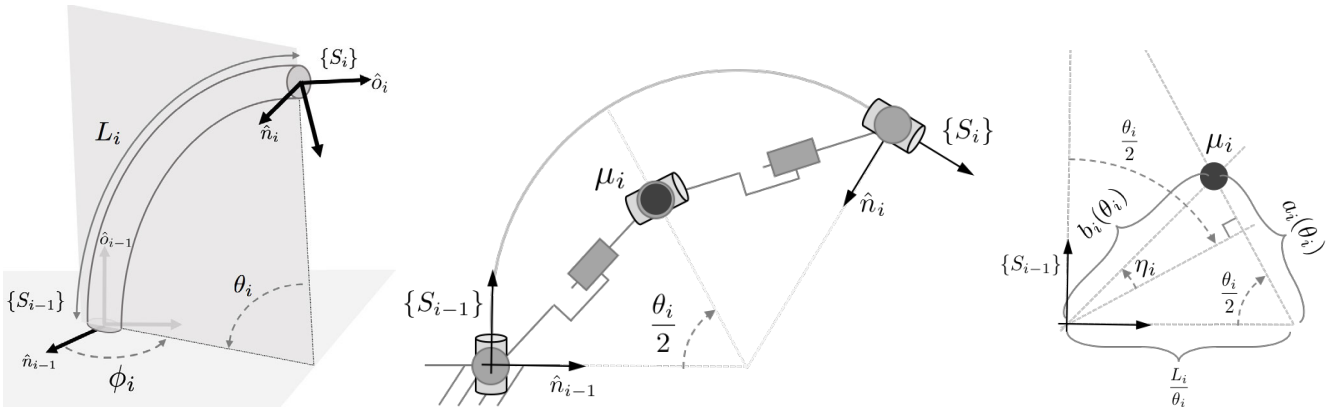

Fig. 3. Kinematic representation of the i-th constant curvature segment. Two local frames are placed at the two ends of the segment, $\{S_{i-1}\}$ and $\{S_i\}$ respectively. The length of the segment is L_i, θ_i is the angle of curvature and ϕ_i is the orientation of the plane in which the curvature occurs.

B. Dynamical Terms

The PCC robot dynamics can be derived by constraining the augmented rigid robot dynamics to evolve on $\xi = m(q)$. To this end, we evaluate the augmented configuration derivatives ξ, $\dot{\xi}$, $\ddot{\xi}$, w.r.t. q, $\dot{q}$, $\ddot{q}$

$$\begin{cases} \xi &= m(q) \\ \dot{\xi} &= J_{\mathrm{m}}(q)\dot{q} \\ \ddot{\xi} &= \dot{J}_{\mathrm{m}}(q,\dot{q})\dot{q} + J_{\mathrm{m}}(q)\ddot{q}\,, \end{cases} \tag{11}$$

where $J_{\mathrm{m}}(q) : \mathbb{R}^n \to \mathbb{R}^{10n\times n}$ is the Jacobian of $m(\cdot)$, i.e. $\frac{\partial m}{\partial q}$. This set of non linear equation is integrable in the augmented formulation dynamics. The resulting dynamics is (please refer to [19] for the detailed derivation)

$$B(q)\ddot{q} + C(q,\dot{q})\dot{q} + G_{\mathrm{G}}(q) = \tau + J^T(q) f_{\mathrm{ext}}\,, \tag{12}$$

where $B \in \mathbb{R}^{n\times n}$ is the PCC robot's inertia matrix, $C \in \mathbb{R}^{n\times n}$ is the centrifugal and Coriolis matrix, $G_{\mathrm{G}} \in \mathbb{R}^n$ is the gravitational field, and $J^T(q)$ maps external forces $f_{\mathrm{ext}} \in \mathbb{R}^n$ into joint torques. These terms are defined as

$$\begin{cases} B(q) &= J_{\mathrm{m}}^T(q)\, B_\xi(m(q))\, J_{\mathrm{m}}(q) \\ C(q,\dot{q}) &= J_{\mathrm{m}}^T(q)\, B_\xi(m(q))\, \dot{J}_{\mathrm{m}}(q,\dot{q}) \\ &\quad + J_{\mathrm{m}}^T(q)\, C_\xi(m(q), J_{\mathrm{m}}(q)\dot{q})\, J_{\mathrm{m}}(q) \\ G_{\mathrm{G}}(q) &= J_{\mathrm{m}}^T(q)\, G_\xi(m(q)) \\ J(q) &= J_\xi(m(q))\, J_{\mathrm{m}}(q) \end{cases} \tag{13}$$

where $B_\xi \in \mathbb{R}^{10n\times 10n}$ is the augmented robot's inertia matrix, $C_\xi \in \mathbb{R}^{10n\times 10n}$ collects Coriolis and centrifugal terms, $G_\xi \in \mathbb{R}^{10n}$ takes into account the effect of gravity on the robot. J_ξ is the Jacobian mapping external wrenches into generalized forces at the joint level. Note that (12) has the form of a classic rigid robot dynamics.

C. Impedance model

We complete (12) by introducing elastic and dissipative terms. It is convenient to directly evaluate the impedance for the PCC soft robot using the configuration variable q, and its derivative $\dot{q}$. We model the elasticity of a link through a continuous and homogeneous distribution of infinitesimal springs and dampers along the cross-sectional area of a segment. We hypothesize here a linear characteristic for each of these elements, and a circular cross-section of the robot. Under these assumptions stiffness and damping matrices of the i-th segment are

$$K_i = \begin{bmatrix} 0 & 0 \\ 0 & k_i \end{bmatrix}, \quad D_i(q) = \beta_i \begin{bmatrix} {\theta_i}^2 & 0 \\ 0 & 1 \end{bmatrix} \tag{14}$$

We do not report here the complete derivation for the sake of space. The full stiffness matrix K and damping matrix $D(q)$ are block diagonal concatenations of K_i and D_i.

D. Actuation

We consider here the system actuated through a set of internal torques, applied along the axes $\hat{x}_i$ and $\hat{y}_i$ of each segment. The resulting input field is $\tau_i = A_i(q_i)\tau_{\mathrm{A},i}$, where

$$A_i(q_i) = \begin{bmatrix} -\cos(\phi_i)\sin(\theta_i) & -\sin(\phi_i) \\ -\sin(\phi_i)\sin(\theta_i) & \cos(\phi_i) \end{bmatrix}. \tag{15}$$

$\tau_i \in \mathbb{R}^2$ are the generalized forces acting directly on ϕ_i and θ_i respectively, as in (16). $\tau_{\mathrm{A},i} \in \mathbb{R}^2$ are instead the torque around the two axes. See experimental section from more details about how these torques can be produced. The full input field $A(q)$ is the block diagonal concatenation of $A_i(q_i)$.

E. Full Model

The resulting model describing the evolution of the soft robot's degree of curvature q in time is

$$\begin{aligned} B(q)\ddot{q} + C(q,\dot{q})\dot{q} + D(q)\dot{q} + G_{\mathrm{G}}(q) \\ + K\,q = A(q)\tau_{\mathrm{A}}\,, \end{aligned} \tag{16}$$

where B, C, G_{G}, J are defined in (12)-(13), K, D in (14), and A in (15). Note that no interactions with the external environment are considered in this work.

IV. Feedback Controller

We propose the following controller for implementing trajectory following in the soft robot's state space q

$$\begin{aligned}\tau_{\mathrm{A}} = A^{-1}(q)(G_{\mathrm{G}}(q) + C(q,\dot{q})\dot{\bar{q}} + B(q)\ddot{\bar{q}} \\ + K\bar{q} + K_{\mathrm{P}}(\bar{q}-q) + D(q)\dot{\bar{q}} + K_{\mathrm{D}}(\dot{\bar{q}}-\dot{q}))\end{aligned} \tag{17}$$

where $q, \dot{q} \in \mathbb{R}^n$ are the curvature vector and its time derivative. $\bar{q}(t), \dot{\bar{q}}(t), \ddot{\bar{q}}(t) \in \mathbb{R}^n$ are the desired evolution and its derivatives expressed in curvature space. $B \in \mathbb{R}^{n\times n}$ is the robot's inertia, $C \in \mathbb{R}^{n\times n}$ is the Coriolis and Centrifugal matrix, $K \in \mathbb{R}^{n\times n}$ is the robot's stiffness matrix. $D : \mathbb{R}^n \to \mathbb{R}^{n\times n}$ is the nonlinear damping. $K_{\mathrm{P}}, K_{\mathrm{D}} \in \mathbb{R}^{n\times n}$ are two control gains. Combining (12) and (17) yields the closed loop dynamics

$$B(q)\ddot{e} + C(q,\dot{q})\dot{e} = -(K + K_{\mathrm{D}})\, e - (D(q) + K_{\mathrm{D}})\dot{e}\ , \tag{18}$$

where $e := \bar{q} - q$ is the tracking error. $A^{-1}(q)$ inverts the input characteristics, enabling the direct combination of corresponding model and the control actions. The term $G_{\mathrm{G}}(q)$ in the controller operates as a direct compensation of the gravity field. The feedforward actions $K\bar{q}$ and $D(q)\dot{\bar{q}}$ are combined with the robot's impedance to produce a physical feedback action. In this way, low feedback gains K_{P}, K_{D} can be used, avoiding a change of the natural softness of the system [23]. It is worth underlining that the resulting dynamics in (18) have a structure similar to the dynamics of a classic rigid robot controlled through a PD controller, with configuration-dependent damping $D(q)+K_{\mathrm{D}}$. The matching between the two dynamics is exact when $\dot{\bar{q}} = 0$. In this case, the convergence can be trivially proven by using standard results in the control of rigid robots. Due to space limitations, we can not provide formal proof of convergence for the general case of $\dot{\bar{q}} \neq 0$, which would follow a similar logic of the one we proposed in [20].

V. State estimation

We consider the estimation of posture q from the posture of each frame $T_{\mathrm{w}}^0, T_0^1, T_0^2, \ldots, T_0^n \in \mathrm{SE}(3)$, as defined in Sec. II. This information is typically provided by commonly used sensors such as motion capture systems or inertial measurement units. First, we derive the local transformation from the global ones

$$T_{i-1}^i = (T_0^{i-1})^{-1} T_0^i\ . \tag{19}$$

Note that in the real application the robot is not going to fulfill the hypothesis of piecewise constant curvature exactly. Therefore, the state estimation algorithms are going to act implicitly as a conversion. For this reason we had to choose carefully the more robust way of extracting ϕ_i and θ_i from T_{i-1}^i. This translated in using as much as possible the position vector t_{i-1}^i, as expressed by the following equations

$$\begin{aligned}\phi_i &= \arctan\left(\frac{t_{i-1}^i[2]}{t_{i-1}^i[1]}\right) \\ \theta_i &= \mathrm{sign}(t_{i-1}^i[3])\,|\arcsin\sqrt{(R_{i-1}^i[1,3])^2 + (R_{i-1}^i[2,3])^2}|\ ,\end{aligned} \tag{20}$$

where $R_{i-1}^i[j,k]$ is the (j,k)-th element of the matrix (3), and $t_{i-1}^i[j]$ is the j-th element of (4).

VI. Simulations

For the sake of space and conciseness we do not report here the simulation results for the nominal case of PCC robot. We instead focus on the use of the discussed control strategy for the control of Soft Robots, of which PCC robots can be considered an approximation, as discussed in the introduction. We use a similar to the one proposed in [24] to simulate the robot. Four actuated segments are considered. Each is discretized in six segments of the same length. Each segment is connected to the subsequent one through two revolute joints as to implement an equivalent of ϕ and θ. On the equivalent θ is connected an elastic element with stiffness $12\frac{\mathrm{Nm}}{\mathrm{rad}}$. On each joint is applied a linear damping of $3\frac{\mathrm{Nms}}{\mathrm{rad}}$. The total length of the soft robot is 1m, and its weight is 1kg, homogeneously distributed along the structure. The parameters of the PCC model are estimated through a step response, in order to reproduce experimental conditions.

We tested the proposed architecture in tracking a trajectory at the end effector. The reference is evaluated on-line by integrating the following Jacobian based inverse kinematics

$$\begin{cases}\dot{\bar{q}} &= J^+(p_{\mathrm{d}}(t) - J\dot{q}) \\ \ddot{\bar{q}} &= \dot{J}^+(\dot{p}_{\mathrm{d}}(t) - \dot{p}) + J^+(\ddot{p}_{\mathrm{d}}(t) + (\dot{p}_{\mathrm{d}} - J\dot{q}))\end{cases} \tag{21}$$

with $p_{\mathrm{d}} \in \mathbb{R}^3$ reference expressed in Cartesian coordinates. We consider as desired trajectory at the end effector the following lemniscate of Gerono

$$p_{\mathrm{d}}(t) = \left[-0.25,\ \ \frac{\cos(\pi t/5)}{3},\ \ -0.5 + \frac{\sin(2\pi t/5)}{6}\right]^{\mathrm{T}} \mathrm{m}\ . \tag{22}$$

Fig. 4 and 5 show the resulting evolution of ϕ and θ respectively. The proposed algorithm proves its robustness in dealing non constant curvature and tilting, converging in few seconds to the trajectory specified by the kinematic inversion. This results even more clearly by looking at the trajectory in Cartesian space, depicted in Fig. 6. Finally Fig. 7 shows the soft robot tracking the prescribed trajectory.

VII. Experiments

In this section, we validate the control algorithm presented in the previous sections through physical experiments on an actual prototype. We start by first describing the fabrication of the proposed soft robotic arm, and explaining the experimental setup. This is followed by the results of our closed-loop control experiments on the physical prototype.

A. Experimental Setup

The experimental setup consists of a soft multi-segment arm as well as the actuation and motion capture system. The arm is presented here for the first time.

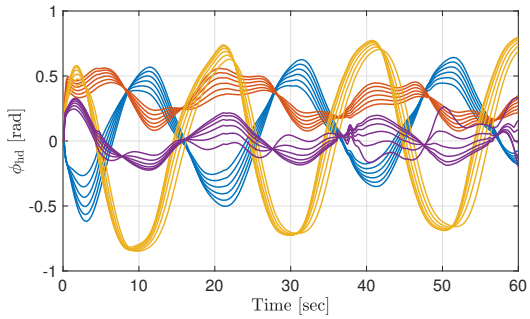

(a)

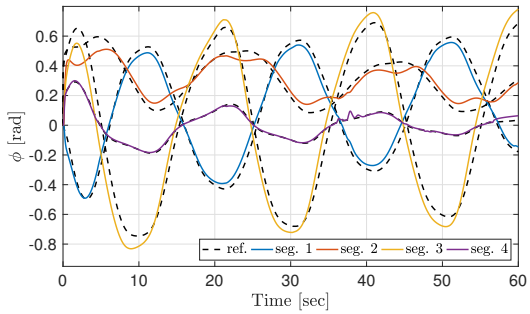

(b)

Fig. 4. Evolution of ϕ variables. Panel (a) shows the evolution of variables in the simulated model, while panel (b) shows corresponding angles in PCC parametrization. The proposed controller is able to track the trajectory despite the discrepancies between the two models.

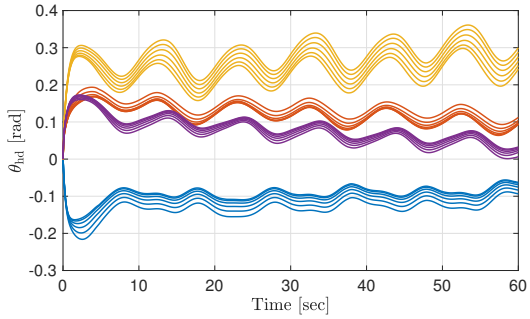

(a)

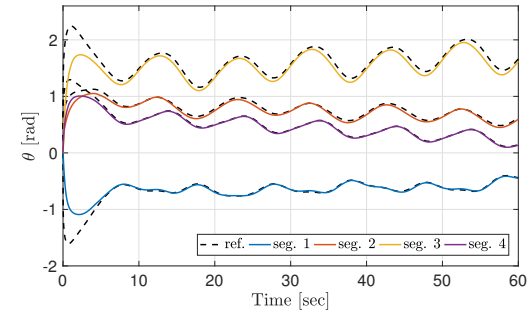

(b)

Fig. 5. Evolution of θ variables. Panel (a) shows the evolution of the simulated model, while panel (b) shows corresponding angles in PCC parametrization. The proposed controller achieves almost perfect tracking after few seconds, despite the discrepancies between the two models.

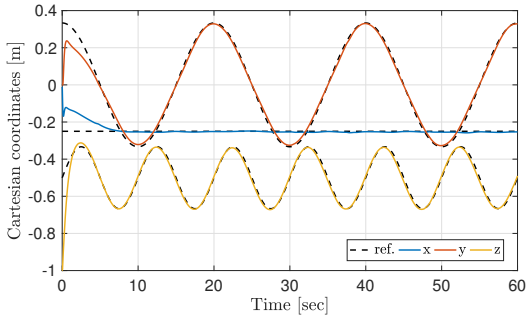

Fig. 6. Tracking of desired trajectory (in dotted lines) at the end effector. The error converges to zero in few seconds.

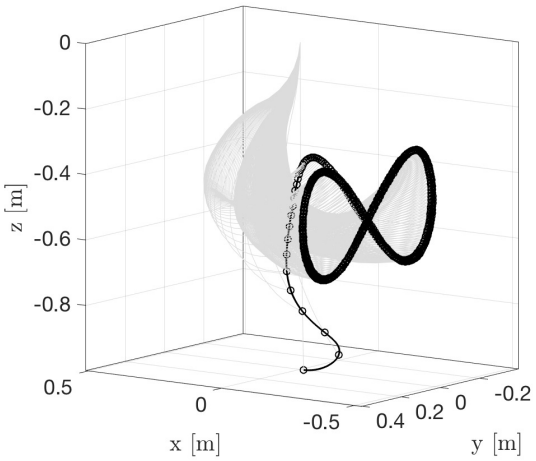

Fig. 7. Graphical representation of of the robot tracking the desired trajectory with its tip.

1) 3D Ribbed Soft Arm: The soft robot presented here is composed of three segments with four inflatable cavities per segment. Each segment of the soft arm is $11\,\mathrm{cm}$ long and has a diameter of $4.5\,\mathrm{cm}$. The manufacturing steps are outlined in Figure 8. The four wax cores are created through injecting liquefied bleached bees-wax into a rubber mold. The wax cores are removed from the mold, post-processed to remove any unnecessary residue, and then assembled into a 3D printed mold for casting a single arm segment. Silicone Rubber is mixed, degassed and filled into the mold. The mold is disassemble and the resulting segment is placed in an oven to melt out the wax and afterwards cooked under boiling water remove any wax residue. Silicone tubing is then glued into one side and silicone rod stock is used to close up the other end of the arm segment. Two more arm segments are manufactured in the same manner. Finally, all silicone tubing is routed so that all three segments can be properly concatenated and glued together. Finally, all tubing is labeled and motion capture markers are added.

2) Actuation and Motion Capture: The independent pneumatic actuation of the arm segments is achieved through an array of 12 pressure-controlled proportional valves. A motion tracking system provides real-time measurements of marked points along the in-extensible back of the soft arm. A rigid

Fig. 8. Overview of the Manufacturing of the 3D Soft Arm Prototype. From Top Left to Bottom Right: Creation of four wax cores through casting; assembly of wax cores into 3D printed molds; casting of Silicone Rubber into the mold; Removal of wax through melting and addition of silicone tubing; Routing of tubing, gluing, labeling and adding markers.

frame holds all the sub-systems together providing reliable hardware experiments without the need for re-calibration of the infrared cameras of the motion capture system.

B. Results of Experimental Validation

1) System Identification: Model (16) has several free parameters: masses μ_i, lengths L_i, stiffnesses k_i, dampings d_i. The first two are evaluated through direct measurements ($0.11\,\mathrm{m}$ and $0.15\,\mathrm{kg}$, respectively), while the latter are estimated from data. We assume same stiffness and damping in all the segments. In addition to the robot's dynamics, we also characterize the behavior of the actuators. The available inputs to our soft robot are the desired pressures of each pneumatic line. The pressures range from $0\,\mathrm{bar}$ to $2\,\mathrm{bar}$. We do not model the actuator's dynamics, but assume it to be a gain α_i, which is an additional variable to be included in the identification. The identification data were collected through four experiments. For each experiment, a step input in pressure is injected into all pneumatic valves actuating one of the four sides of the arm. The amplitudes of the steps were $0.2\,\mathrm{bar}$, $0.4\,\mathrm{bar}$, $0.6\,\mathrm{bar}$, respectively. We hypothesized the same stiffness and damping for each segment in order to reduce the search space for the identification procedure. The remaining seven parameters were identified as the ones minimizing the $2-$norm of the error between estimated and measured evolutions. For this regression problem we used the pseudo-inverse to achieve this goal. The identified stiffness $\hat{k}_i$ is $0.626\,\mathrm{N\,m}$. The damping $\hat{d}_i$ is $0.029\,\mathrm{N\,m\,s}$. The actuator parameters are $\hat{\alpha} = 10^{-3}0.839\mathrm{bar\,N^{-1}\,m^{-1}}$ for each.

2) Posture Tracking: We validate here the ability of (17) to control the proposed soft robot. The gains are set as follows

$$\begin{aligned} K_\mathrm{P} &= \mathrm{diag}(1.2, 0, 1.1, 0, 1, 0)\frac{\mathrm{Nm}}{\mathrm{rad}} \\ K_\mathrm{D} &= \mathrm{diag}(0.002, 0, 0.002, 0, 0.002, 0)\frac{\mathrm{Nms}}{\mathrm{rad}}\,, \end{aligned} \tag{23}$$

where with $\mathrm{diag}(a_1, \ldots, a_6) \in \mathbb{R}^{6\times 6}$ we indicate the diagonal matrix with $a_1, \ldots, a_6$ as diagonal elements. The considered trajectory is

$$\begin{aligned} \bar{\phi}_1(t) &= \pi + \cos(2t), \\ \bar{\phi}_2(t) &= \pi + \cos(2t + \frac{\pi}{3}), \\ \bar{\phi}_3(t) &= \pi + \cos(2t + \frac{2\pi}{3}), \\ \bar{\theta}_1(t) = \bar{\theta}_2(t) = \bar{\theta}_3(t) &= \begin{cases} 0.2 - 0.2\cos(\pi t), & t \leq 1\,\mathrm{s}. \\ 0.4, & \text{otherwise}. \end{cases} \end{aligned} \tag{24}$$

Note that due to the high softness of the system, constant trajectories are very difficult to maintain during the wide, out-of-phase oscillations imposed at ϕ.

Fig. 9 presents the resulting evolutions. The controller shows very good tracking performance on the first two segments, while the quality decreases at the third segment. Since this behaviour does not manifest in simulated experiments, we believe that it could be connected to defect in the fabrication of the third segment.

VIII. Conclusion

In this work, we presented a closed-loop control approach, that can equip soft robots with the ability of tracking trajectories in 3D space. Nevertheless, the experimental results still leave room for improvements in tracking performance. Our current parametrization of a segment uses a rotational ϕ and a curvature state variable θ. A representation singularity arises when θ is close to 0 or when ϕ switches from π to $-\pi$. A more suitable parametrization avoiding is worthwhile investigating. The control methodology used in this work is based on a constant curvature model describing a one dimensional arc. This approach does not scale once the length dimension of the arm is not anymore much larger than the radial dimension of the arm. Also, a non-uniform radius along a segment and the ribbed shape of the interior cavities make the material heterogeneous, which is not captured by the model.

Acknowledgment

This research was conducted in the Distributed Robotics Laboratory at MIT with support from the National Science Foundation (grant NSF 1830901 and NSF 1226883). We are grateful for this support.

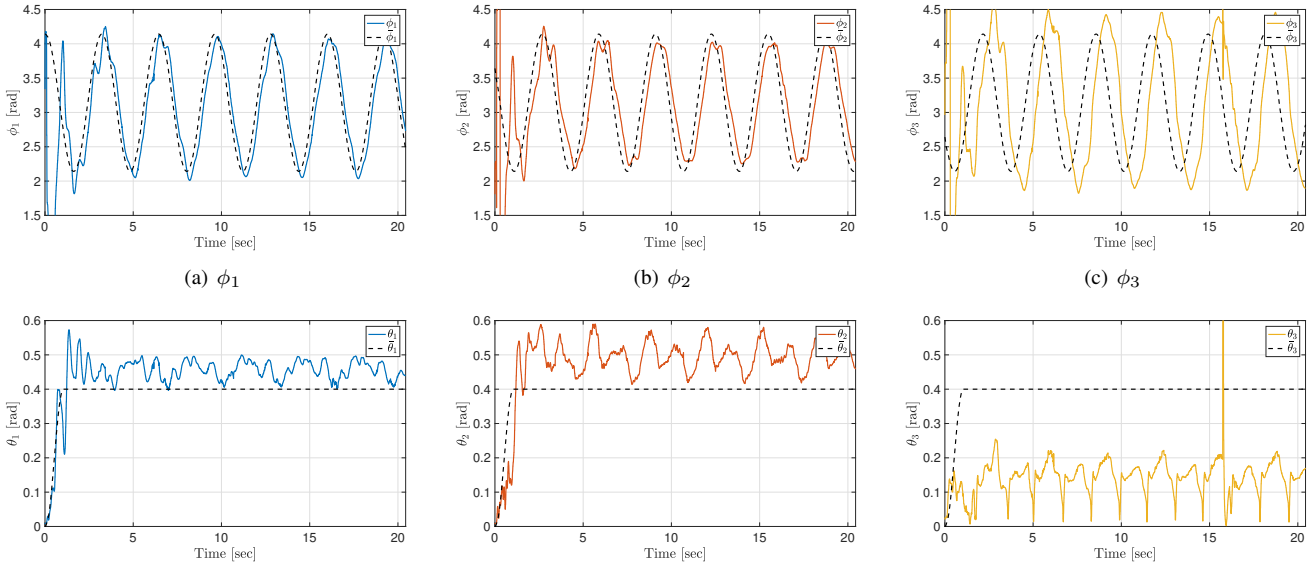

(a) ϕ_1 (b) ϕ_2 (c) ϕ_3

(d) θ_1 (e) θ_2 (f) θ_3

Fig. 9. Experimental trajectories resulting from the application of controller (17) to track (24).

REFERENCES

[1] D. Rus and M. T. Tolley, "Design, fabrication and control of soft robots," *Nature*, vol. 521, no. 7553, pp. 467–475, 2015.

[2] R. Deimel and O. Brock, "A novel type of compliant and underactuated robotic hand for dexterous grasping," *The International Journal of Robotics Research*, vol. 35, no. 1-3, pp. 161–185, 2016.

[3] C. Laschi, M. Cianchetti, B. Mazzolai, L. Margheri, M. Follador, and P. Dario, "Soft robot arm inspired by the octopus," *Advanced Robotics*, vol. 26, no. 7, pp. 709–727, 2012.

[4] R. K. Katzschmann, J. DelPreto, R. MacCurdy, and D. Rus, "Exploration of underwater life with an acoustically controlled soft robotic fish," *Science Robotics*, vol. 3, no. 16, 2018. [Online]. Available: http://robotics.sciencemag.org/content/3/16/eaar3449

[5] P. Polygerinos, N. Correll, S. A. Morin, B. Mosadegh, C. D. Onal, K. Petersen, M. Cianchetti, M. T. Tolley, and R. F. Shepherd, "Soft robotics: Review of fluid-driven intrinsically soft devices; manufacturing, sensing, control, and applications in human-robot interaction," *Advanced Engineering Materials*, 2017.

[6] D. Trivedi, A. Lotfi, and C. D. Rahn, "Geometrically exact models for soft robotic manipulators," *IEEE Transactions on Robotics*, vol. 24, no. 4, pp. 773–780, 2008.

[7] Z.-H. Luo, B.-Z. Guo, and Ö. Morgül, *Stability and stabilization of infinite dimensional systems with applications*. Springer Science & Business Media, 2012.

[8] M. Giorelli, F. Renda, G. Ferri, and C. Laschi, "A feed-forward neural network learning the inverse kinetics of a soft cable-driven manipulator moving in three-dimensional space," in *Intelligent Robots and Systems (IROS), 2013 IEEE/RSJ International Conference on*. IEEE, 2013, pp. 5033–5039.

[9] T. G. Thuruthel, E. Falotico, M. Manti, and C. Laschi, "Stable open loop control of soft robotic manipulators," *IEEE Robotics and Automation Letters*, vol. 3, no. 2, pp. 1292–1298, 2018.

[10] Z. Zhang, J. Dequidt, A. Kruszewski, F. Largilliere, and C. Duriez, "Kinematic modeling and observer based control of soft robot using real-time finite element method," in *Intelligent Robots and Systems (IROS), 2016 IEEE/RSJ International Conference on*. IEEE, 2016, pp. 5509–5514.

[11] A. Lismonde, V. Sonneville, and O. Brüls, "Trajectory planning of soft link robots with improved intrinsic safety," *IFAC-PapersOnLine*, vol. 50, no. 1, pp. 6016–6021, 2017.

[12] R. J. Webster III and B. A. Jones, "Design and kinematic modeling of constant curvature continuum robots: A review," *The International Journal of Robotics Research*, vol. 29, no. 13, pp. 1661–1683, 2010.

[13] G. Runge and A. Raatz, "A framework for the automated design and modelling of soft robotic systems," *CIRP Annals-Manufacturing Technology*, 2017.

[14] S. H. Sadati, S. E. Naghibi, I. D. Walker, K. Althoefer, and T. Nanayakkara, "Control space reduction and real-time accurate modeling of continuum manipulators using ritz and ritz–galerkin methods," *IEEE Robotics and Automation Letters*, vol. 3, no. 1, pp. 328–335, 2018.

[15] F. Renda, F. Boyer, J. Dias, and L. Seneviratne, "Discrete cosserat approach for multi-section soft robots dynamics," *arXiv preprint arXiv:1702.03660*, 2017.

[16] S. Grazioso, G. Di Gironimo, and B. Siciliano, "A geometrically exact model for soft continuum robots: The finite element deformation space formulation," *Soft robotics*, 2018.

[17] V. Falkenhahn, A. Hildebrandt, R. Neumann, and O. Sawodny, "Model-based feedforward position control of constant curvature continuum robots using feedback linearization," in *Robotics and Automation (ICRA), 2015 IEEE International Conference on*. IEEE, 2015, pp. 762–767.

[18] A. D. Marchese, R. Tedrake, and D. Rus, "Dynamics and trajectory optimization for a soft spatial fluidic elastomer manipulator," *The International Journal of Robotics Research*, vol. 35, no. 8, pp. 1000–1019, 2016.

[19] C. Della Santina, R. K. Katzschmann, A. Bicchi, and D. Rus, "Dynamic control of soft robots interacting with the environment," *Proceedings of the 1st IEEE Conference of Soft Robots*, 2018.

[20] ——, "Model-based dynamic feedback control of a planar soft robot: trajectory tracking and interaction with the environment," *Under review at Internation Journal of Robotics Research*, 2019.

[21] L. Sciavicco and B. Siciliano, *Modelling and control of robot manipulators*. Springer Science & Business Media, 2012.

[22] B. A. Jones and I. D. Walker, "Kinematics for multisection continuum robots," *IEEE Transactions on Robotics*, vol. 22, no. 1, pp. 43–55, 2006.

[23] C. Della Santina, M. Bianchi, G. Grioli, F. Angelini, M. Catalano, M. Garabini, and A. Bicchi, "Controlling soft robots: balancing feedback and feedforward elements," *IEEE Robotics & Automation Magazine*, vol. 24, no. 3, pp. 75–83, 2017.

[24] R. S. Penning and M. R. Zinn, "A combined modal-joint space control approach for continuum manipulators," *Advanced Robotics*, vol. 28, no. 16, pp. 1091–1108, 2014.